Journal of Geodynamics 65 (2013) 292–307

Contents lists available at SciVerse ScienceDirect

Journal of Geodynamics

journal homepage: http://www.elsevier.com/locate/jog

Kinematics of Sürgü Fault Zone (Malatya, Turkey): A remote sensing study

Ayten Koç*, Nuretdin Kaymakcı

Department of Geological Engineering, Middle East Technical University, Ankara 06531, Turkey

ARTICLE INFO

Article history:
Received 11 January 2012
Received in revised form 3 August 2012
Accepted 4 August 2012
Available online 13 August 2012

Keywords:
Strike-slip fault
Remote sensing
Palaeostress analysis
Fault kinematics
SE Anatolia

ABSTRACT

The Sürgü Fault Zone (SFZ) is located in SE Anatolia extending from Göksun in the west to Çelikhan in the east, where it bifurcates from the East Anatolian Fault Zone. A detailed analysis along the fault using satellite images, digital elevation models (DEMs) and aerial photographs revealed that the SFZ displays characteristic deformation patterns common to dextral strike-slip faults, including pressure ridges, displaced linear valleys, and deflected stream courses. In addition to this, fault slip data collected from 17 sites indicated that the SFZ is a dextral strike-slip fault zone having reverse and normal components in its western and eastern parts, respectively. The type of dip-slip components, orientation of the palaeostress configurations, and related structures along the fault are compatible with along strike variations of a strike-slip fault system that supports the dextral nature of the fault zone. Observed maximum cumulative stream deflections along the fault zone indicate that the dextral offset of the SFZ has been more than 3 km since the establishment of the stream network in the region. According to the preferred tectonic model suggested in this study, the present dextral motion along the SFZ occurs within a regional sinistral system related to westwards escape of the Maraş Block, squeezed between Anatolian Block and Arabian Plate in N–S direction.

1. Introduction

The structural deformation patterns in strike-slip fault zones have been established since the 1980s (Biddle and Christie-Blick, 1985; Sylvester, 1988). Strike-slip fault zones are classified as convergent, divergent and simple or through-going strike-slip faults, depending on the movement vectors of intervening blocks (Sanderson and Marchini, 1984). In simple strike-slip zones, the major horizontal compression axis makes an approximately 45° angle with the zone (Fig. 1a) while this angle is higher in the convergent strike-slip faults and in divergent strike-slip fault zones it is less than 45° (Sanderson and Marchini, 1984). Development of convergent and divergent strike-slip fault zones depends on the change in the regional stress field or reactivation of zones of weakness (Dewey et al., 1995). Analog and numerical models (Wilcox et al., 1973; Segall and Pollard, 1983) demonstrated that the pattern of structures within strike-slip fault zones is controlled by the type and orientation of horizontal major and minor compressive stresses as well as along strike variations of the master fault strand (Ambraseys and Tchalenko, 1970; Biddle and Christie-Blick, 1985; Woodcock and Fischer, 1986; Sylvester, 1988). In a strike-slip fault zone, the master fault strand (MFS), which is also known as the principal displacement zone (PDZ), or y-shear (Fig. 1a) develops generally at an advanced stage of strike-slip displacement, parallel to the main shear zone (Naylor et al., 1986). The other structures include Synthetic Shear (or r-shear), Antithetic Shear (r′-shear), Secondary Synthetic Shear (p-shear), extension structures (normal faults, gashes), and compressional en-echelon folds and high angle reverse faults (Fig. 1a). The r-, and p-shears are sub-parallel (approximately ±15°) to the y-shear and they all have the same sense of slip. However, the angle between the y-shear and the r′-shear is around 75° and they have opposite slip senses (Fig. 1a). The angular relationship between the structures is mainly controlled by the internal friction angle of the faulted material and the cohesion and they obey the Coulomb–Mohr criterion (Jaeger and Cook, 1971).

The East Anatolian Fault Zone (EAFZ) is one of the major sinistral intra-continental strike-slip faults in Eastern Anatolia along which the Anatolian Block is moving westwards (Şengör and Yılmaz, 1981) (Fig. 1b). The EAFZ displays all the characteristic features of a sinistral strike-slip fault zone (Perinçek et al., 1987; Perincek and Çemen, 1990; Lyberis et al., 1992), and recent GPS studies indicate that the fault zone is transferring the total convergent vector into strike-slip motion (Reilinger et al., 2006), which implies that overall EAFZ is a simple (through-going) strike-slip fault zone without convergence nor divergence. On the other hand, a number of splay faults bifurcate from the main strand of the EAFZ and transfer the deformation out of the fault zone. Fault kinematic (e.g. Arpat and Şaroğlu, 1972; Şaroğlu et al., 1992; Perinçek et al., 1987;

* Corresponding author.
E-mail addresses: kayten@metu.edu.tr (A. Koç), kaymakci@metu.edu.tr (N. Kaymakcı).

0264-3707/$ – see front matter © 2012 Elsevier Ltd. All rights reserved.
http://dx.doi.org/10.1016/j.jog.2012.08.001

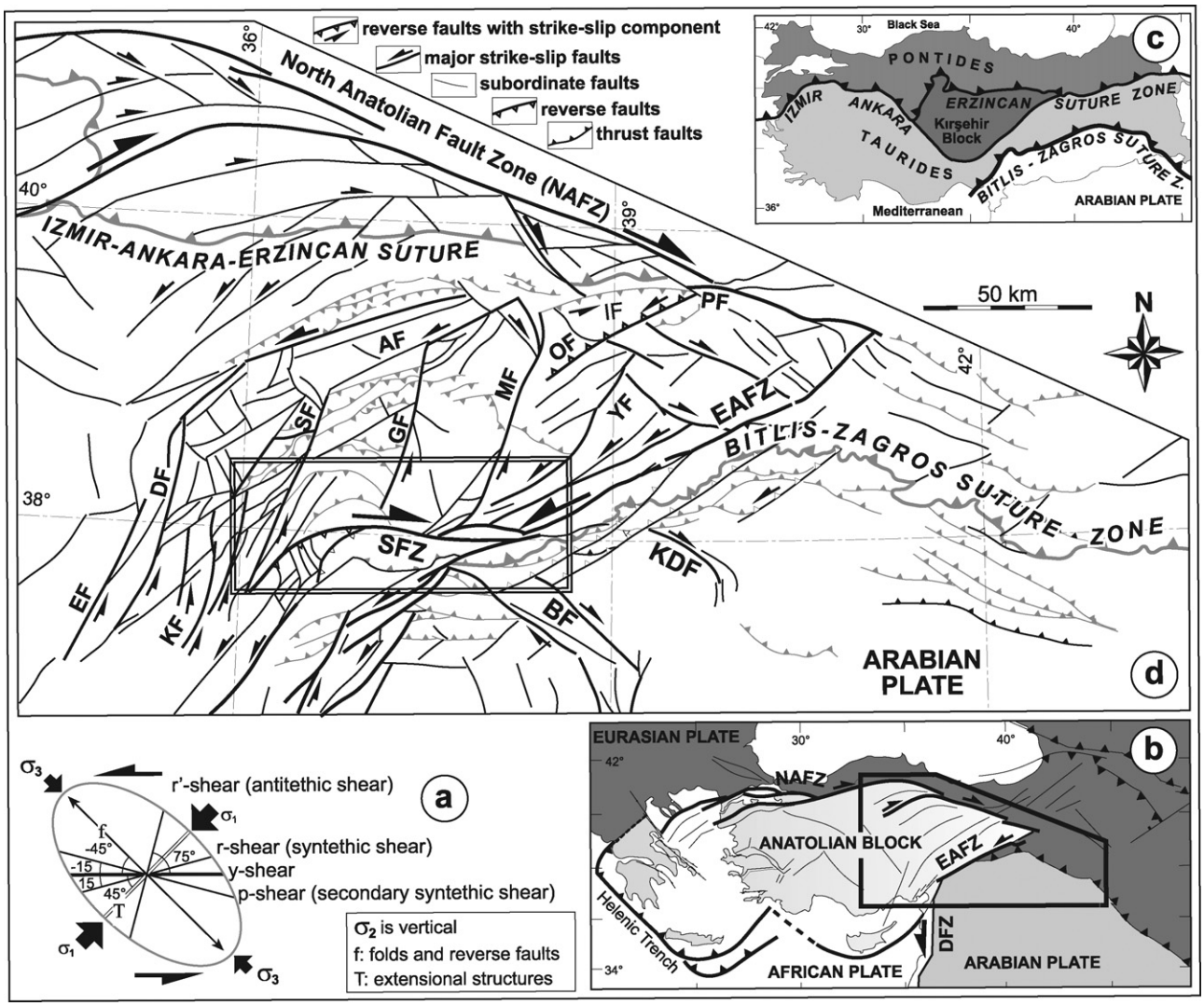

Fig. 1. (a) Riedel deformation pattern terminology for a sinistral shear zone (after Ambraseys and Tchalenko, 1970; Sylvester, 1988), (b) major active structures around eastern Mediterranean, (c) major paleotectonic units of Turkey (modified from Şengör and Yılmaz, 1981), (d) major paleotectonic and active structures in central and SE Anatolia (after Kaymakci et al., 2010). AF: Altınyayla Fault, BF: Bozova Fault, DF: Develi Fault, DFZ: Dead Sea Fault Zone, EAFZ: East Anatolian Fault Zone, EF: Ecemiş Fault, GF: Gürün Fault, IF: Iliç Fault, KDF: Karcadağ Fault, KF: Kozan Fault, NAFZ: North Anatolian Fault Zone, MF: Malatya Fault, OF: Ovacık Fault, PF: Pertek Fault, SF: Sarız Fault, SFZ: Sürgü Fault Zone, YF: Yeşilyurt Fault.

Perincek and Çemen, 1990; Lyberis et al., 1992; Kaymakci et al., 2010 and references there in) and GPS studies (e.g. Reilinger et al., 2006) indicate most of these splay faults are reactivated older structures which do not necessarily obey Coloumb–Mohr deformation criterion. Sürgü Fault Zone (SFZ) is one of the splay faults which bifurcates from EAFZ around Çelikhan with approximately E–W strike and the bifurcation angle is about 30° (Fig. 1d). Morphotectonic features and fault kinematic data indicate that the SFZ is a dextral strike-slip fault zone contrary to expected sinistral sense proposed by previous studies (Arpat and Şaroğlu, 1975; Perinçek and Kozlu, 1984). This makes the SFZ a peculiar structure as being a dextral fault zone sub-parallel to a major sinistral intra-continental EAFZ. Such motion along the SFZ seems not to be feasible according to published analog and numerical models and most of the field observations elsewhere. Therefore, the dextral nature of the SFZ deserves explanation.

In this context, the main purpose of this study is to determine the geometry, deformation mechanism and kinematics of the SFZ by using remote sensing techniques and field studies including fault slip measurements. Additionally, it is aimed to construct a tectonic model in order to provide a satisfactory explanation for the controversial behavior of the SFZ. For these purposes, various image processing and enhancement techniques were applied to data sources including Landsat TM, ETM+, Quickbird and ASTER imagery combined with SRTM and 1/25,000 scale digital elevation models, and stereo-pairs of aerial photographs. The results obtained from remotely sensed data have been verified in the field. During the field verification, fault slip data were collected and detailed observations of the structures were performed.

2. Geological setting

The Late Cretaceous to recent tectonic development of the eastern Mediterranean region is related to the convergence between the Afro-Arabian and Eurasian plates, which is mostly accommodated by northward subduction of branches of the Neotethys Ocean (Şengör and Yılmaz, 1981; Barrier and Vrielynck, 2008) leading to the formation of two major suture zones (Fig. 1c). These include the northern and southern branches of the Neotethys Ocean (Şengör and Yılmaz, 1981). The northern one is demarcated by the Izmir-Ankara-Erzincan Suture Zone and developed between the Pontides (Eurasia) in the north and Tauride-Anatolide Platform (Gondwana)

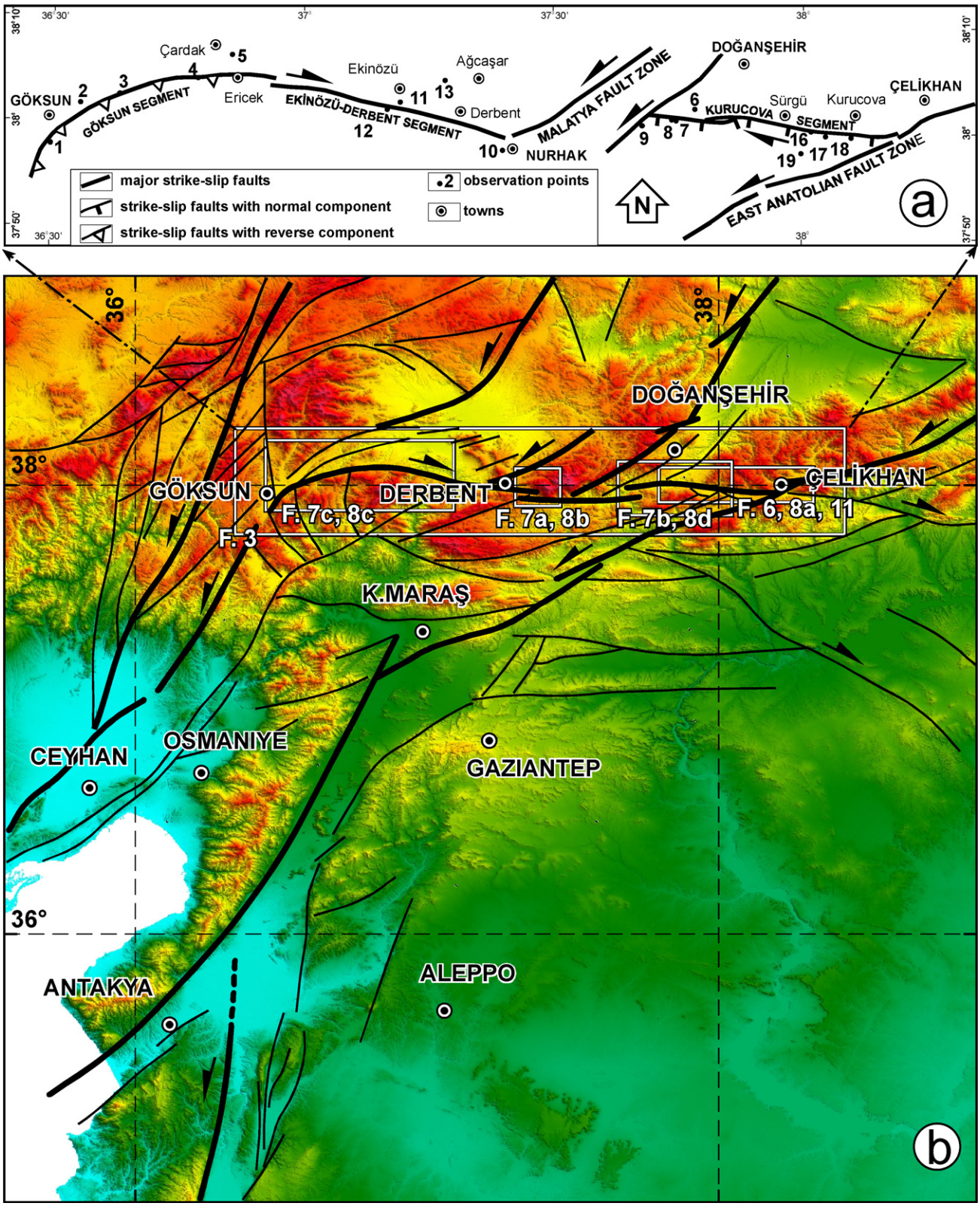

Fig. 2. (a) Sample locations and (b) major tectonic elements in the vicinity of the study area (legend is like in Fig. 1) (after Perinçek et al., 1987; Kaymakci et al., 2006, 2010).

in the south (Fig. 1c). The intervening continental blocks collided after the oceanic lithosphere was completely subducted northwards under the Pontides by the end of the Late Cretaceous and collision lasted until the end of the Oligocene to Earliest Miocene (Kaymakci et al., 2001, 2003, 2009). The southern branch is demarcated by the Bitlis Zagros Suture Zone and developed due to collision between the Arabian Plate and the Eurasian Plate (Fig. 1c) by the Eocene to Oligocene (Ghasemi and Talbot, 2005; Hüsing et al., 2009; Rolland et al., 2012) or later, by the end of Middle Miocene (Şengör and Yılmaz, 1981; Dewey et al., 1986; Keskin, 2003; Şengör

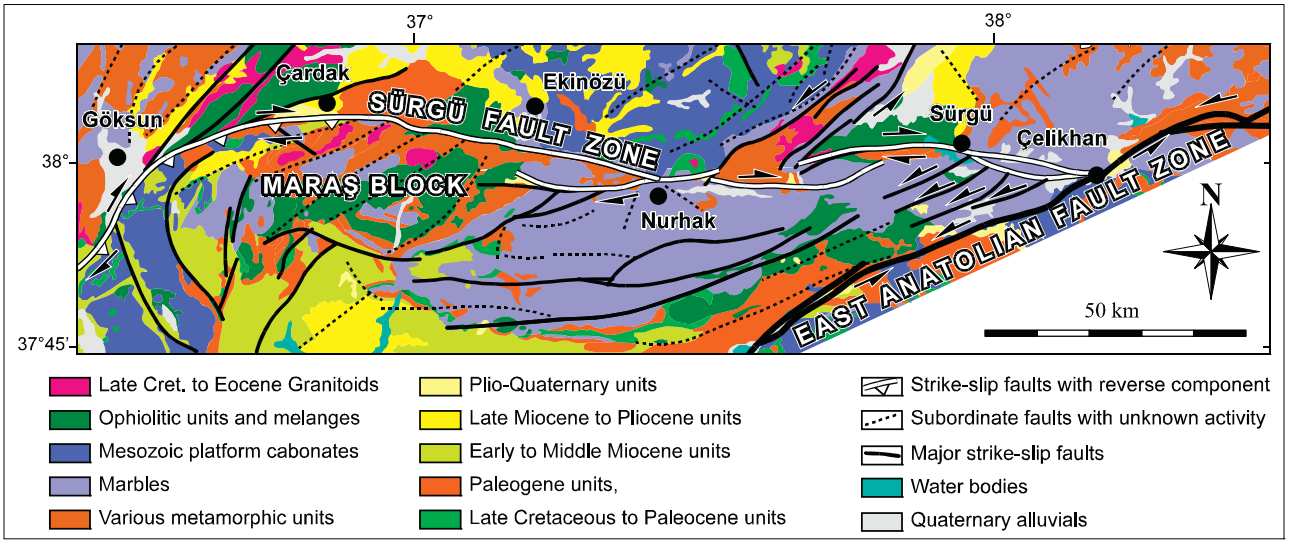

Fig. 3. Simplified geological map and active faults of the study area (partly modified from 1/500,000 scale geological map of MTA). Half arrows indicate direction of fault block movements.

et al., 2003; Faccenna et al., 2006; Hüsing et al., 2009; Okay et al., 2010).

Although the exact timing of collision between Eurasian and Arabian plates is still under debate, the consequences of this collision are better known Nevertheless, post-collisional convergence in eastern Anatolia is still active and gave way to the development of transcurrent tectonics that is dominated by the dextral North Anatolian and sinistral East Anatolian fault zones. Along these fault zones, the Anatolian Block is escaping westwards toward the Hellenic trench (Fig. 1b) which accommodate Africa-Eurasian convergence together with Cyprus subduction zone (Şengör et al., 1985; Şengör, 1987; Dewey and Sengör, 1979; Arpat, 1972; Arpat and Şaroğlu, 1975; Khair and Tsokas, 1999).

Apart from Arabian collision, the present tectonic scheme of southern and south-eastern Anatolia has been shaped by subduction of the oceanic lithosphere of the African plate below the Taurides that probably had been subject to slab roll-back, slab detachment, slab break-off and Subduction Transform Edge Propagator (STEP) (Govers and Wortel, 2005) fault processes since the Middle Miocene (Faccenna et al., 2006; Gans et al., 2009; Kaymakci et al., 2010; Van Hinsbergen et al., 2010; Biryol et al., 2011). This resulted in the development of compressional–contractional geodynamics in eastern Anatolia that is manifested by thrusting and strike-slip faulting with considerable reverse components. Westwards, the compressional–contractional deformation in eastern Anatolia has been gradually replaced by strike-slip and extensional tectonics in response to these mantle processes, that dominate mainly in central Anatolia and in western Anatolia respectively (Şengör et al., 1985; Dewey et al., 1986; Perinçek et al., 1987; Şengör, 1987; Reilinger et al., 2006). The end result is a complex array of faults and fault zones that have changed character in space and time since the Middle Miocene. For example, in central and south-eastern Anatolia, three types of faults have developed (Fig. 1d) (Kaymakci et al., 2010). These include: (1) sinistral strike-slip faults with NNE–SSW to NE–SW strike, (2) curvilinear faults with average E–W strike and (3) dextral strike-slip faults with NW–SE strike. At present most of these strike-slip faults have normal or reverse components. The most important factors governing normal or reverse component along a strike-slip fault are their orientation and curvature with respect to main displacement zone and regional stress tensor. For example, re-straining or releasing bends or off-sets accommodate local contraction and extension (Biddle and Christie-Blick, 1985; Sylvester, 1988; Cunningham and Mann, 2007).

The SFZ (Arpat and Şaroğlu, 1975; Perinçek and Kozlu, 1984) has a very peculiar characteristic in having an almost E–W trend (Fig. 2). The fault zone bifurcates from the EAFZ in the east and delimits a number of NNE–SSW trending major faults including Sarız Fault (SF), Gürün Fault (GF), and Malatya Fault (MF) (Fig. 1d). It is almost perpendicular to the N–S convergence vector between the Arabian and Eurasian plates (Reilinger et al., 2006) and has morphotectonic features and kinematic data indicating dextral strike-slip nature with reverse (in the west) and normal (in the east) components; however, it is sub-parallel to the sinistral EAFZ (Fig. 2). This makes the SFZ an enigmatic structure in having a dextral strike-slip character within a sinistral strike-slip setting. This is unexpected since its strike deviates only 30° counter clock-wise from the strike of the EAFZ; hence, it is not an antithetic structure of the EAFZ. Most of the western segment of the SFZ developed along the southern boundary of the Maraş Block (Fig. 3), which contains magmatic arc-massif and Supra Subduction Zone ophiolites developed during the Late Cretaceous to Eocene between the Tauride-Anatolide Platform in the north and Afro-Arabian Plate in the south (Fig. 1c) (Robertson et al., 2006; Kaymakci et al., 2010),

The SFZ and palaeotectonic (pre-Late Miocene) evolution of the region has been studied mainly by Arpat (1972), Arpat and Şaroğlu (1975), Perinçek and Kozlu (1984), Perinçek et al. (1987), Kozlu (1987), Muehlberger and Gordon (1987), Şaroğlu et al. (1992), Yurtmen et al. (2002), and Robertson et al. (2006). However, the geometry, morphotectonics, deformation mechanism and kinematics of the SFZ is still unclear and the discrepancy between its dextral nature and expected sinistral displacement is under debate.

Geographically, the regional extent of the SFZ lies between the Göksun–Çelikhan, Doğanşehir and Nurhak regions where different Mesozoic to Paleogene tectonic units collided and were amalgamated during the Neogene (Fig. 3). The geological map of the region was prepared mainly by Turkish Petroleum Co. geologists during the early 1980s (Perinçek and Kozlu, 1984) and also covered by the 1/500,000 scale Sivas and Hatay sheets of the geological map of Turkey compiled by General Directorate of Mineral Research and Exploration (Ankara, Turkey) (Fig. 3). However these maps are mainly concentrated on lithostratigraphic and large scale structures that do not include most of the active structures.

3. Data and methods

This study integrates data sets obtained from two different disciplines: (1) remote sensing and (2) field observation. Morphotectonic structures and kinematic indicators were mapped and interpreted using remote sensing techniques and subsequently they were verified in the field. Additionally, fault-slip data were collected from mesoscopic faults during field studies for palaeostress inversion analysis.

3.1. Remote sensing analysis

The applied remote sensing techniques included processing and interpretation of satellite images, and stereographic aerial photographs with the utilization of mirror stereoscopes. The used satellite imagery included Landsat 4, 5 and 7 (TM and ETM+), Advanced Space-borne Thermal Emission Radiometer (ASTER), and Quickbird images obtained from Google Earth and 167 stereographic aerial photographs with 1/35,000 scale taken by General Command of Mapping (Turkey). Further image enhancement techniques, including contrast enhancement, color composites, Principal Component Analysis (PCA) and Decorrelation Stretching (DS) were performed on the ASTER and Landsat data in order to enhance image visualization. Additionally, 90 m × 90 m (3″) resolution Shuttle Radar Topographical Mission (SRTM) data and 25 m resolution digital elevation models (DEMs) prepared from 1/25,000 scale topographic maps are used to aid the interpretations. The above mentioned images and DEMs have different levels of spatial (ground) and spectral (i.e., different wavelength) resolutions, and they are useful for distinguishing lithologies and for delineating structures at different scales. Finally, all of these data were co-registered and combined in a GIS environment together with previously obtained maps to carry out an integrated analysis.

3.2. Ground truthing and fault slip data analysis

Field studies were mainly carried out on the main strand of the SFZ for ground truthing of the structures and kinematic indicators interpreted from the remotely sensed imagery in various scales. During the field studies, various compressional and extensional structures were observed in different locations along the fault zone (Fig. 4a and b) in addition to slickensided surfaces (Fig. 5), block tilting (i.e., rotation with respect to horizontal axis), aligned mineral water springs, narrow linear valleys, and fault rocks (phacoids, fault breccia, cataclasites, fault gouge, etc.).

Further, the fault slip data collected from exposed fault planes (Fig. 5) along the main strand of the SFZ were used for stress inversion to resolve the kinematics of the fault zone using Angelier's method (Angelier, 1994). This is based on the reconstruction of the stress ellipsoid in order to determine relative magnitudes and orientations of the principle stresses (Angelier, 1979, 1984, 1990). There are two fundamental assumptions in this approach: (1) the bulk state of stress in a small area is uniform and (2) the slip direction is parallel to the maximum resolved shear stress along an optimally oriented plane of weakness (Wallace, 1951; Bott, 1959). During the construction of the stress configurations, the maximum shear stress direction is determined by calculating the shape factor and orientation of the stress ellipsoid by using the best-fitting reduced stress tensor based on the given fault slip data and the orientations of the three principal stress axes (σ_1: maximum, σ_2: intermediate and σ_3: minimum). The shape factor of any stress ellipsoid is determined from; $\Phi = (\sigma_2 - \sigma_3)/(\sigma_1 - \sigma_3)$ and ranges between two extreme values of 0 and 1. The Φ constraints all-possible cases between uniaxial ($\sigma_2 = \sigma_3$; $\Phi = 0$ or $\sigma_1 = \sigma_2$; $\Phi = 1$) to tri-axial stress configurations ($\sigma_1 > \sigma_2 > \sigma_3$; $\Phi = 0.5$) (Angelier, 1994).

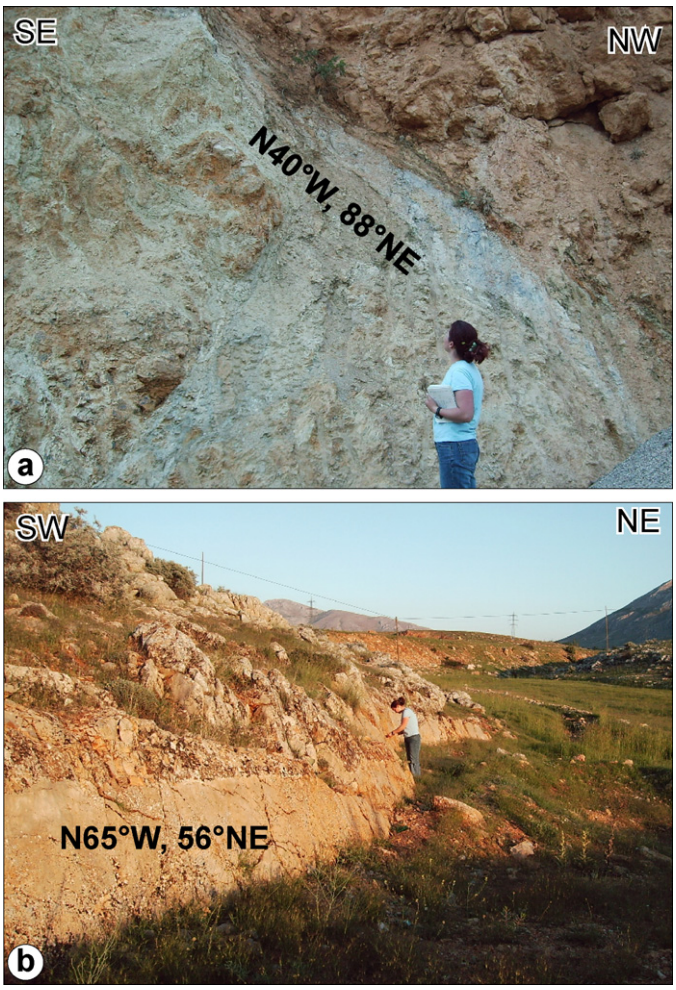

Fig. 4. Field photographs of faults. (a) Intensely sheared reverse fault around site 4 (view to S) and (b) normal faults around site 19 (view to NW) (see Fig. 2a for the locations of the sites).

A total of 246 fault slip measurements were taken from 17 sites across the SFZ. During the analysis of the fault slip data, misfit faults within each analyzed cluster were separated from the bulk data based on maximum misfit angle (ANG) and maximum quality estimator (RUP) and then analyzed separately. This process was applied iteratively until reliable results were obtained. The criteria of the reliability are determined as 20° for the maximum deviation (ANG) and 50° for the maximum value of the quality estimator (RUP) for all the faults in each data set in accordance with the method (Angelier, 1988, 1994). The faults that did not fulfill these conditions were considered as spurious (19 data) and they were disregarded from further analysis and make up around 8% of all data. Inversion of the data was carried out on the remaining 227 slip measurements.

4. Results and discussion

The enhanced satellite images of the Sürgü Fault Zone (SFZ) display various kinematic indicators and morphological features related to its activity. The most prominent of these are the linearly arranged pressure ridges formed mainly along the Kurucaova segment (Fig. 6a), and step-overs along the main course of the SFZ. Pressure ridges are associated with strike-slip motion and controlled by initial fault geometry. In addition, the orientation of the pressure ridges clearly defines the strike of the SFZ, which is mainly in an E–W direction. It starts from the Çelikhan Basin in the east and continues to the Sürgü Village in the west, and controls the

Fig. 5. Reverse fault developed in the western end of the SFZ around Göksun (site 1, see Fig. 2 for its location). (a) Slickensided fault surface (view to SW), (b) its close-up picture, and (c) palaeostress configuration of these faults. Note NW–SE directed compression.

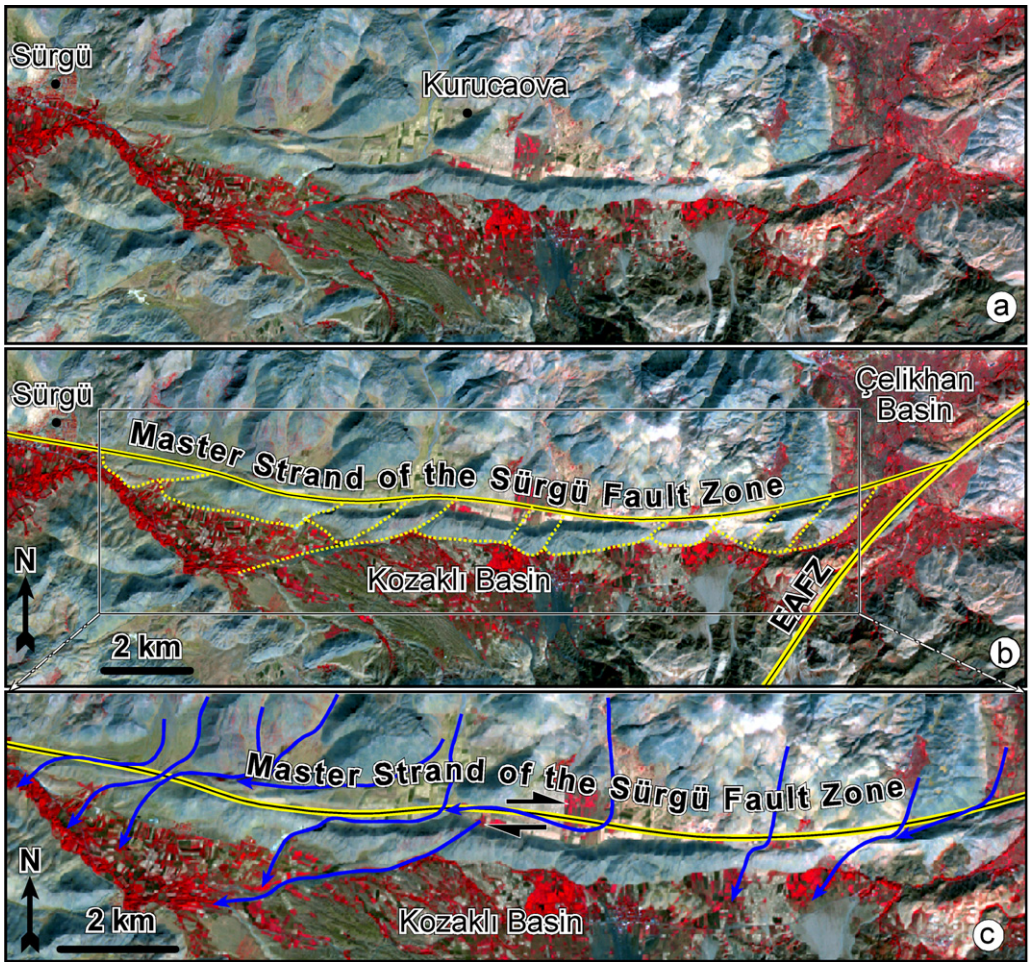

Fig. 6. (a) Uninterpreted and (b) interpreted ASTER image (band combination; R:3, G:2, B:1) showing pressure ridges within an anastomosing pattern of faults (yellow lines), EAFZ: East Anatolian Fault Zone. (c) ASTER image (band combination; R:3, G:2, B:1) showing dextrally displaced streams along the SFZ between Çelikhan Basin and Sürgü Village. (For interpretation of the references to color in this figure legend, the reader is referred to the web version of the article.)

northern margin of the Kozaklı Basin (Fig. 6b). Within the zone of pressure ridges, a number of deflected streams with apparent dextral offset are also observed (Fig. 6c). Maximum observed deflections in the stream courses reach up to 3 km (Fig. 6c). Similarly, displaced streams are also detected NW of Nurhak and east of Derbent (Fig. 7a). However, the deflection pattern is more complex and non-uniform, unlike the deflections observed in the Kozaklı Basin. In that part of the SFZ, some of the stream channels do not have clear downstream continuations and this may be due to contortion of the drainage. This results in fanning out of stream courses that do not yield a visible channel course. Therefore, the maximum observed dextral displacement around Derbent is approximately 1 km (Fig. 7a).

Remote sensing analysis also provided information from different lithologies by processing and enhancement of spectral information. The juxtaposition of different lithologies is the diagnostic criterion for determination of fault traces and their offset. For example, a number of different lithologies are juxtaposed along the central segment of the SFZ on a very sharp trace and result in a very prominent color contrast in the ASTER images due to their differing petrography and mineralogy (Fig. 7b). On the other hand, at its western part, the different segments of the SFZ are easily recognized due to abrupt changes in elevation on linear scarps and cliffs. In this area, the high topography of the southern block tectonically limits the alluvial plain of the Göksun and Elbistan basins. Along this segment, the main course of the SFZ is bent gradually southwards (Fig. 7c).

Aerial photographs used in this study allowed a 3D visualization capability and facilitated verification of the detected lineaments and geomorphological features observed on the satellite images such as long linear ridges (Fig. 8a), sudden relief changes, stream course deflections (Fig. 8b) or truncations (contortions) and disturbed stream network (Fig. 8c). The pressure ridges (which are also shutter ridges along the Kurucaova segment of the SFZ) and the deflected streams in the northern margin of the Kozakli Basin (Fig. 8a) and in the east of Derbent and northwest of Nurhak (Fig. 8b) are clearly visible and recognizable in the aerial photographs and Quickbird images (Fig. 8d) with the deflection magnitudes just as observed on the ASTER images. Moreover, the belt of pressure ridges can be divided into a number of small blocks bounded by NE–SW striking en echelon faults with sinistral off-set, and displays an anastomosing pattern supporting

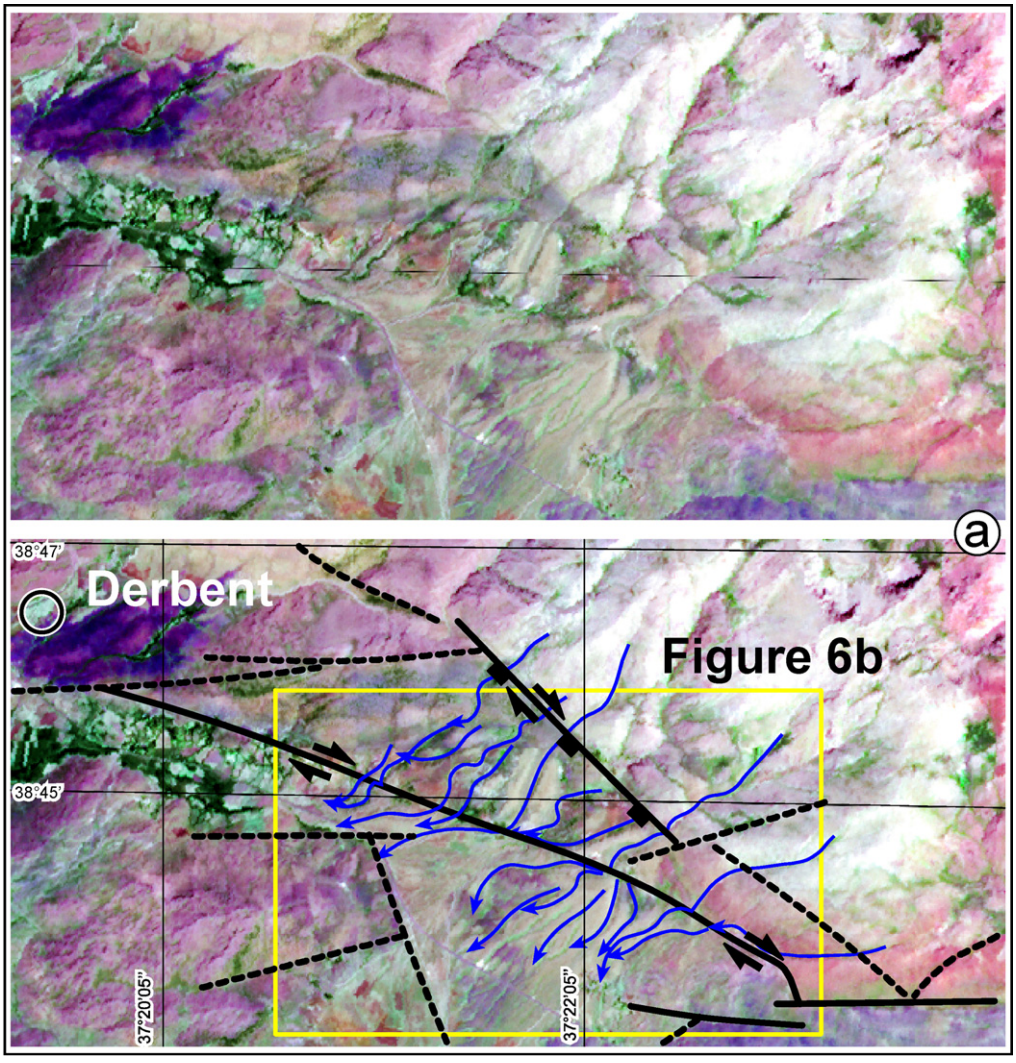

Fig. 7. Original and interpreted images from Sürgü Fault Zone. (a) Deflected streams along the SFZ in around Derbent overlaid on ASTER image. Band combinations RGB:5,2,1 with saturation enhancement (see Fig. 2 for its location) (yellow box indicates the position of Fig. 6b). (b) Master strand of the SFZ near Sürgü Dam indicated with white arrows and overlaid on decorrelation stretched (DS) ASTER image. Band combinations; RGB:4,2,1. Note very sharp trace of the master strand of the SFZ. (c) Subset of an ASTER image depicting a very sharp trace of the western part of the SFZ (for the sake of simplicity fault trace is not delineated but indicated with arrows). The image is produced by DS and Principal Component Analysis (PCA). Band combination; RGBI:5,3,1, intensity is PC-1. (For interpretation of the references to color in this figure legend, the reader is referred to the web version of the article.)

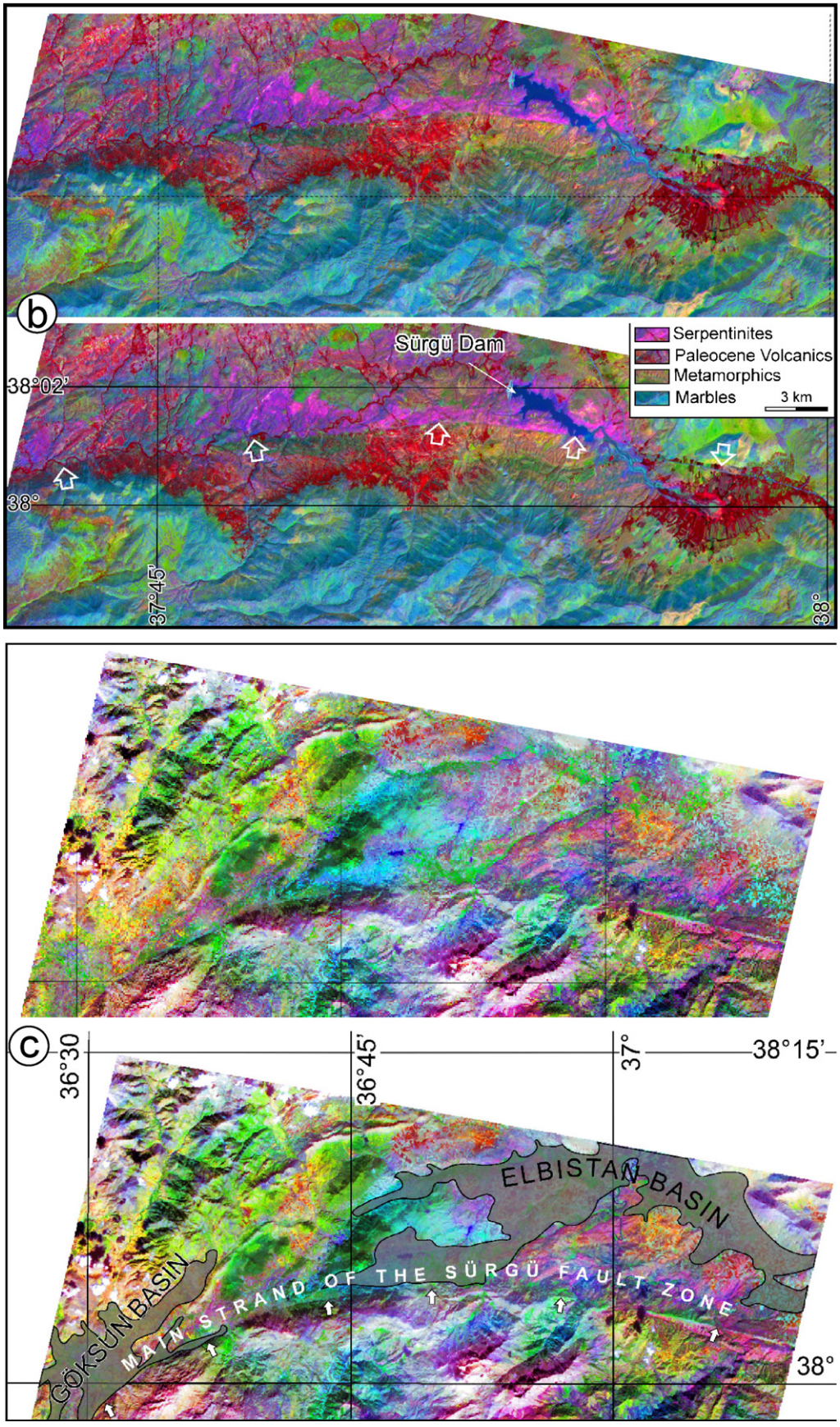

Fig. 7. (*Continued*).

clockwise block rotations along the dextral Kurucaova segment (Fig. 8a).

In the west, relief information extracted from the aerial photographs indicates a sudden elevation change and abutting of the southern block of the SFZ to the alluvial plain of Göksun Basin (Fig. 8c). This section is characterized by the sharp north dipping main strand of the SFZ and a number of NE–SW trending en-echelon folds. Since these folds were developed within pre-Neogene units which pre-date the SFZ, they are not taken into consideration, even though they have compatible orientations with the dextral movement of the SFZ and may indicate paleotectonic movement sense of the fault zone. This has further implications, such that during the paleotectonic period the fault zone was also a dextral strike-slip fault zone that reactivated during the neotectonic period co-axially or it kept its slip sense since then.

The host lithologies of the collected fault slip data range from Paleozoic to Mesozoic marbles and metamorphics, to Late Cretaceous ophiolites and ophiolite related units, to Paleocene volcanic and clastic units, and to Neogene sedimentary and volcanic units (Fig. 3). The fault slip data on the pre-Cenozoic units may belong

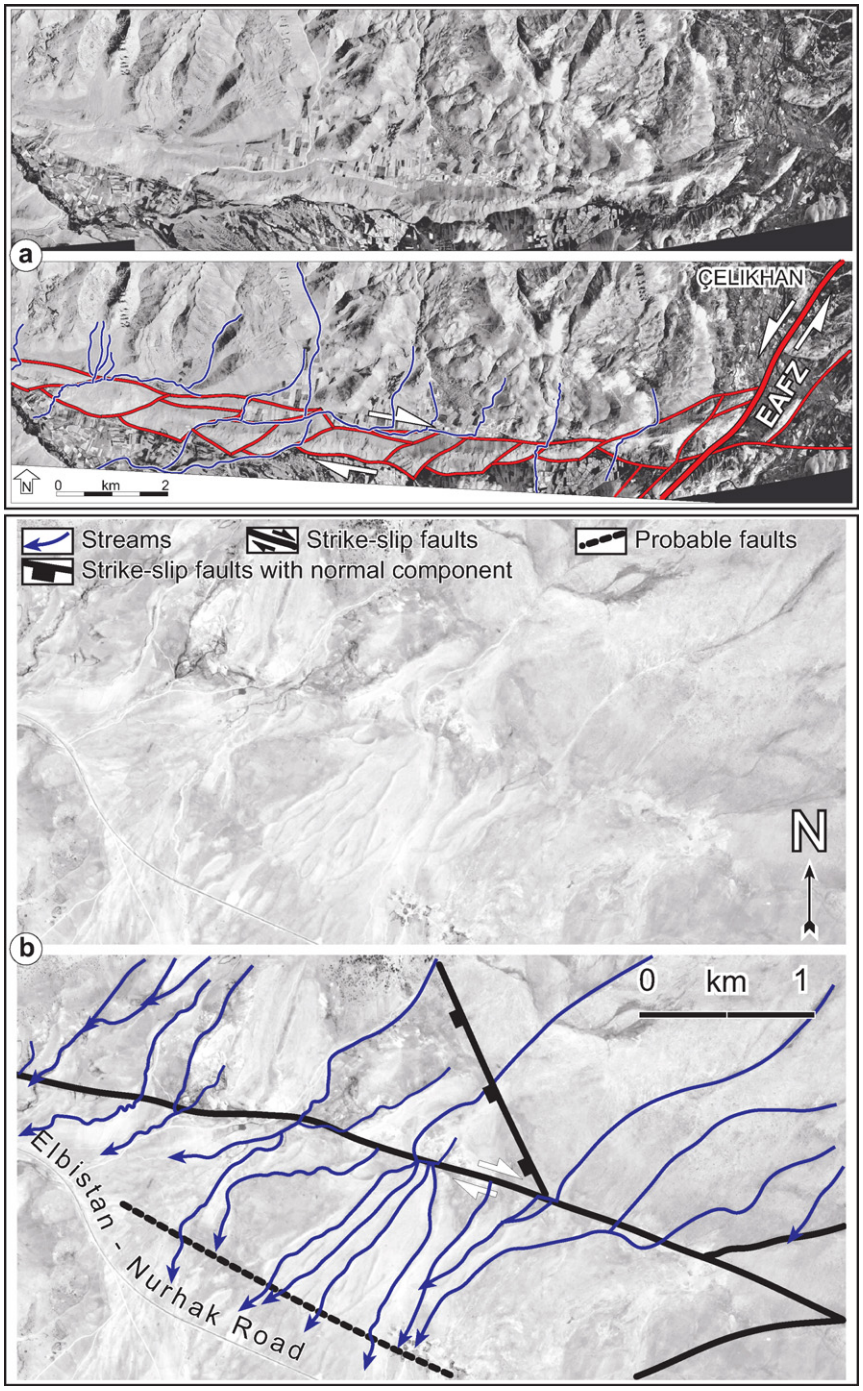

Fig. 8. Original an interpreted images from Sürgü Fault Zone. (a) Aerial photo showing pressure ridges within an anastomosing pattern of faults (red) and dextrally displaced stream courses (blue). EAFZ: East Anatolian Fault Zone. Note that all the streams flow southwards. (b) Deflected streams in E of Derbent and NW of Nurhak overlaid on the aerial photo (see Fig. 5b for its location). (c) Aerial photo showing western part of the study area. Main strand of the SFZ is dipping northwards and is indicated with red arrows. Singly plunging anticlines and synclines are indicated with yellow lines. Divergent white arrows are alluvial fans. (d) Quickbird image (obtained from Google Earth) indicating dextrally deflected stream. (For interpretation of the references to color in this figure legend, the reader is referred to the web version of the article.)

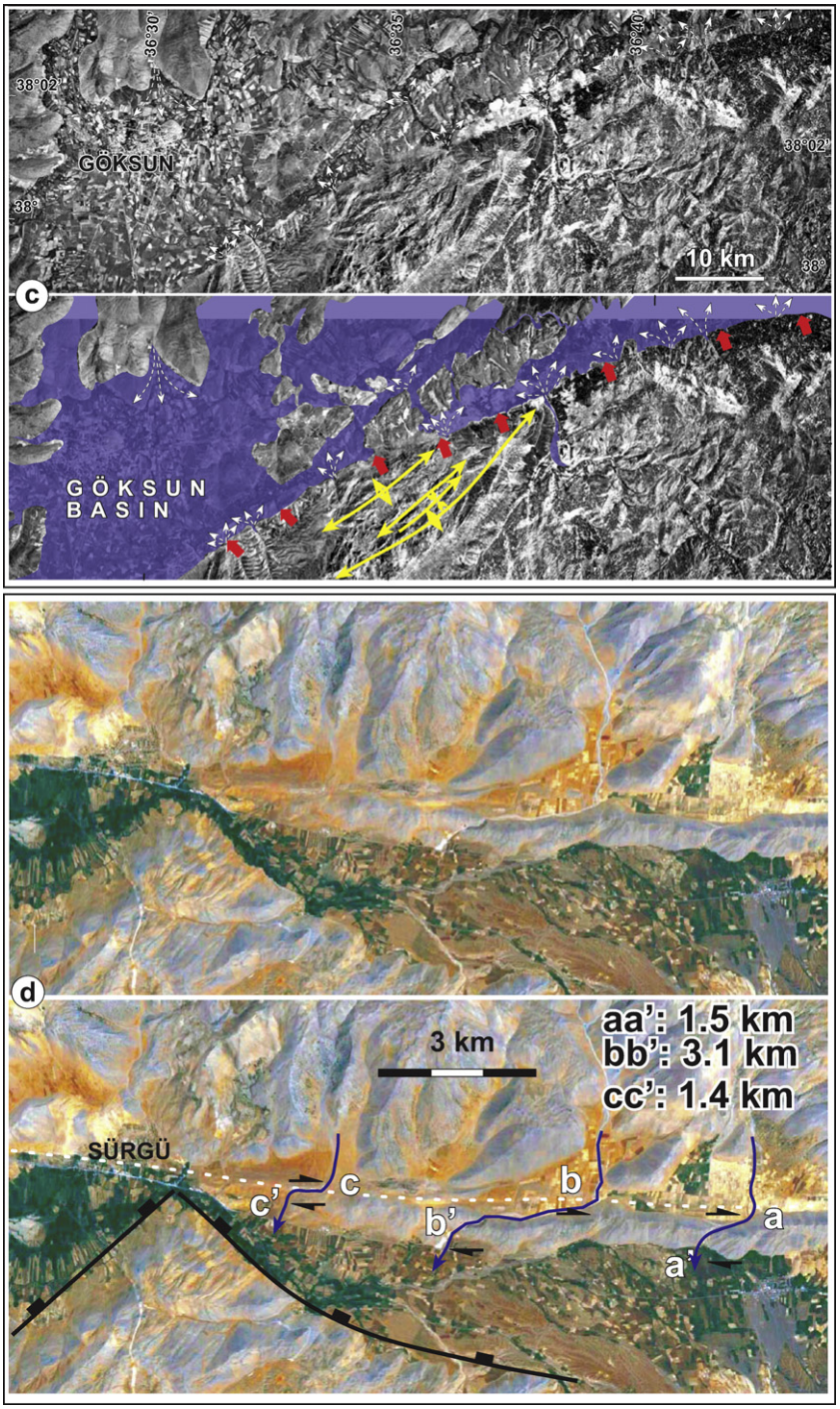

Fig. 8. (*Continued*).

to both past and present deformation phases. However, adjacent Quaternary basins partly juxtaposed by the fault itself indicate current activity that is consistent with the slip data. For example, the fault zone thrust over the Quaternary units close to western end (near sites 1–4), around SE of Göksun (Fig. 5). Similarly, the fault juxtaposes the Quaternary units laterally along the Kurucaova segment where the fault plane displays clear striations. Based on these observations, fault slip data collected from fresh surfaces of the fault plane, in contact with Quaternary deposits, have been associated with the latest phase of deformation along the Sürgü Fault Zone.

Extracted stress configurations shown in Fig. 9 and Table 1 indicate that the major principal stress (σ_1) is generally oriented (sub-) horizontally, whereas σ_2 and σ_3 are interchangeably sub-vertical (oblique) in all sites except sites 9 and 19 (Fig. 9a) where σ_1 is vertical. This is characteristic for triaxial stress conditions where Φ values are close to 0.5 (Table 1). In addition, oblique orientations of principal stresses characterize a triaxial strain condition that deviates greatly from Andersonian (Anderson, 1951) types of faults (Reches, 1978, 1983; Krantz, 1988).

The horizontal components of the constructed stress configurations are plotted in order to understand the style of deformation and to check compatibility of the constructed principal stress directions, and to assess the nature of local and regional structures. Apart from some extensional solutions (sites 9 and 19), the horizontal component of most of the σ_1 directions at each site make an approximately 45° angle with the local trend of the SFZ and they

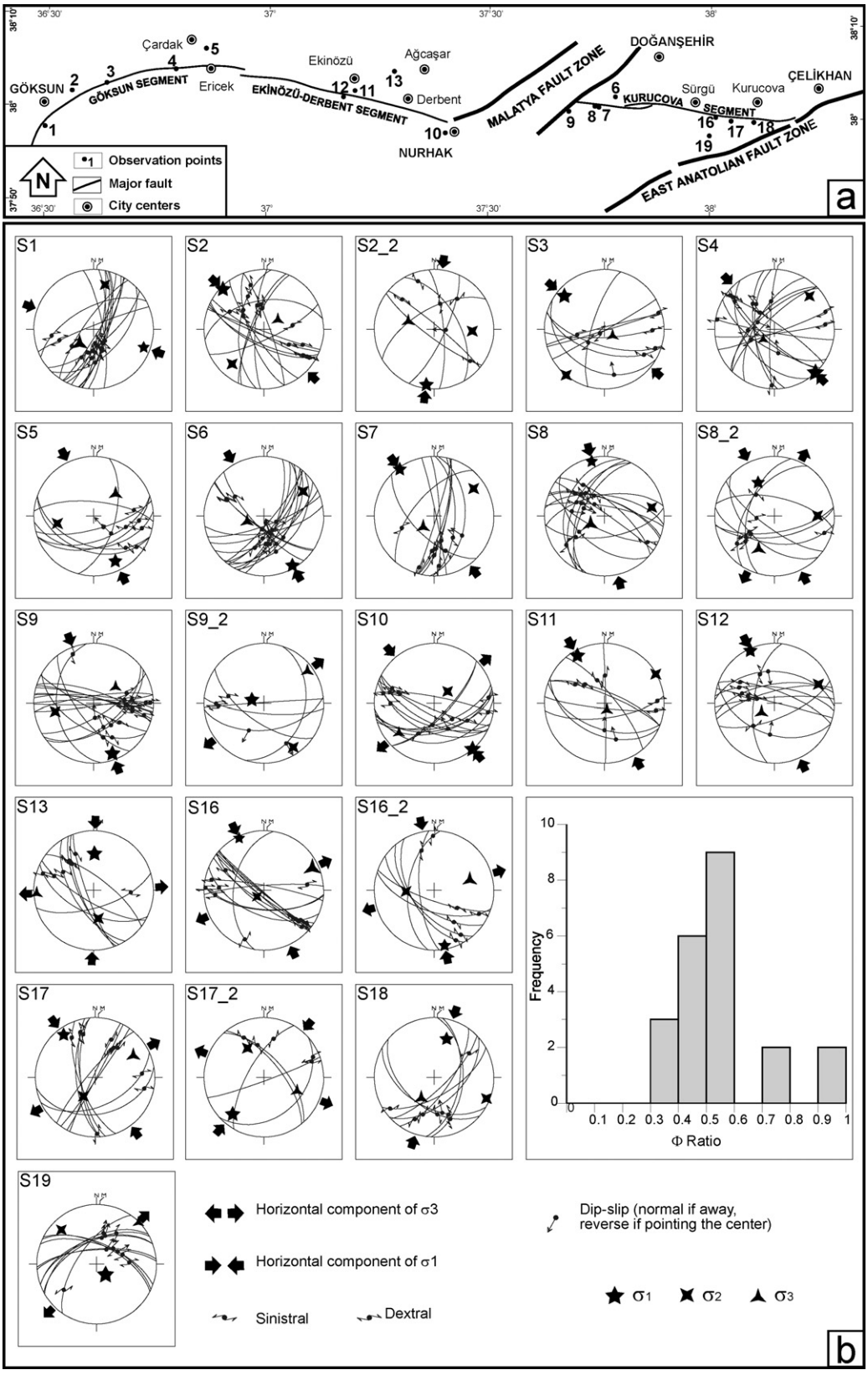

Fig. 9. (a) Locations of the palaeostress measurements and (b) Cyclographic traces of fault planes and constructed palaeostress configurations for each site (lower hemisphere, equal area projection) and frequency distributions of Φ values.

Table 1
Locations and palaeostress orientations for whole data.

Loc	Lattitude	Longitude	σ_1(P°/D°)	σ_2(P°/D°)	σ_3(P°/D°)	Φ	Mean ANG	Mean RUP	N
S1	37.96489	36.49892	12°/110°	24°/014°	62°/224°	0.901	10	36	15
S2	37.98370	38.00130	05°/314°	22°/222°	67°/056°	0.402	13	40	14
S2_2	37.98370	38.00130	7°/188°	36°/093°	53°/287°	0.547	15	45	6
S3	38.03013	36.55727	14°/287°	00°/081°	76°/195°	0.454	21	53	8
S4	38.04186	36.63613	0°/137°	47°/063°	228°/153°	0.449	15	49	15
S5	38.07265	36.79154	18°/154°	38°/259°	47°/045°	0.564	12	41	8
S6	38.10761	36.85804	05°/150°	23°/058°	66°/252°	0.599	15	34	16
S7	38.03726	37.78788	03°/324°	21°/55°	69°/225°	0.590	14	40	10
S8	38.01855	37.74778	07°/347°	20°/79°	68°/240°	0.720	16	41	14
S8_2	38.01855	37.74778	39°/337°	28°/093°	38°/207°	0.592	9	48	7
S9	37.99261	38.10045	12°/160°	35°/258°	53°/054°	0.513	15	40	17
S9_2	37.99261	38.10045	73°/285°	13°/146°	11°/054°	0.457	19	50	5
S10	38.01959	37.74177	00°/140°	66°/049°	24°/230°	0.449	19	49	13
S11	37.99579	38.04844	10°/330	01°/061°	80°/158°	0.410	19	51	8
S12	38.01014	37.68138	04°/335	21°/067°	68°/235°	0.563	16	40	10
S13	37.96834	37.40117	39°/001°	51°/171°	5°/267°	0.368	7	26	8
S16	38.04039	37.19666	78°/227°	04°/335°	12°/065°	0.913	15	35	13
S16_2	38.04039	37.19666	07°/169°	51°/268°	38°/074°	0.545	13	40	7
S17	38.02951	37.17252	12°/324°	59°/212°	27°/060°	0.762	7	34	10
S17_2	38.02951	37.17252	20°/220°	43°/331°	40°/112°	0.408	14	16	5
S18	38.07745	37.28425	33°/018°	06°/112°	56°/212°	0.559	14	55	8
S19	38.00276	37.99653	71°/140°	19°/314°	02°/045°	0.317	13	30	10

$\sigma_1, \sigma_2, \sigma_3$: magnitude ratios of principle stresses; D/P: direction/plunge; Φ: stress ratio; ANG: maximum allowed angular divergence; RUP: maximum allowed quality value; N: number of measurement for each site.

are orthogonal to the observed folds, especially in the western part of the fault zone (Fig. 10).

Fig. 10 shows smoothed trajectories of the principal planes that are based on stress inversion results to give an impression about the spatial distribution of the stress field over the area. These trajectories were created manually based on the intersection of the horizontal plane with principal planes. The orientation of maximum principle stress (σ_1) is taken as the reference direction since σ_2 and σ_3 are interchangeable and are generally sub-vertical or sub-horizontal. It is important to note that the deviation of the maximum stress (σ_1) orientation is gradual and changes from NW–SE in the west to N–S in the east, which is compatible (Biddle and Christie-Blick, 1985; Sylvester, 1988) with the bending of the Sürgü Fault Zone from west to east.

4.1. Kinematic of Sürgü Fault

As previously mentioned, the Sürgü Fault Zone was first recognized by Arpat and Şaroğlu (1975) and they claimed that it is a left lateral strike-slip fault bifurcated from the EAFZ. Later Perinçek and Kozlu (1984) and Perinçek et al. (1987) delineated and mapped the fault zone; at the same time they also described general characteristics of the major active faults in eastern Turkey. Recent activity of the SFZ was briefly discussed in these studies and the authors claimed that the SFZ comprises a single through-going sinistral fault, rather than a fault zone. Westaway et al. (2006) further speculated that the Sürgü Fault Zone took up the sinistral displacement between the Anatolian and Arabian plates in the Eastern Anatolia during the Pliocene. However, palaeostress configurations and the observations documented in this paper show that Sürgü Fault Zone is a dextral strike-slip fault zone, which has a reverse component in the west especially along the Göksun segment; on the other hand, it has normal components especially along the Kurucaova segment in the east. This is manifested by various structural and kinematic indicators such as fault slip data and dextrally deflected drainage. In addition, it is observed that there are number of NE–SW oriented blocks delimited by very prominent fault traces with normal components in the southern margin of the Kozaklı Basin (Fig. 11a). The

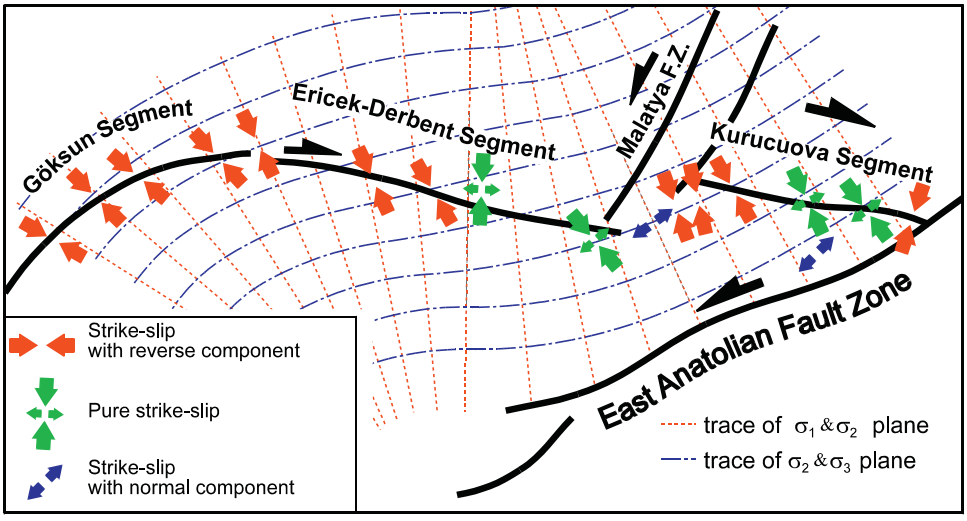

Fig. 10. The spatial distribution of horizontal components of constructed palaeostress configurations, segments of the SFZ and trajectories of horizontal components of σ_1–σ_2 and σ_2–σ_3 planes.

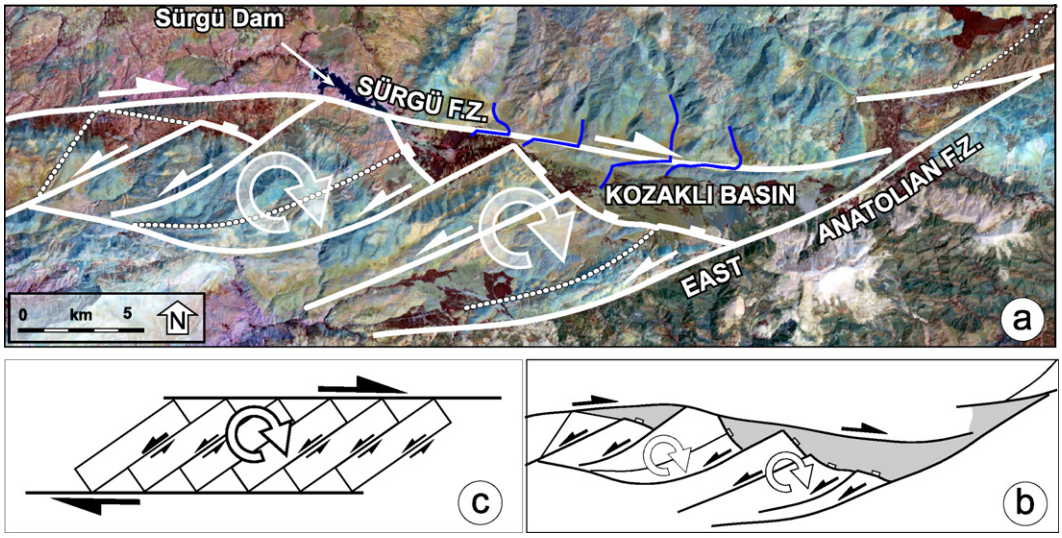

Fig. 11. Fault blocks developed in the eastern part of the SFZ. Background image is Landsat TM image (band combination RGB:5,3,1). (b) Simplified map of showing only the faults and basins (grey) fault. (c) Domino style (bookshelf) faulting proposed for the development of fault blocks along the SFZ. Note sinistral movement (half arrows) of clockwise rotating blocks (circular arrows) within dextral system (SFZ). Note also that all faults are not indicated for the sake of simplicity.

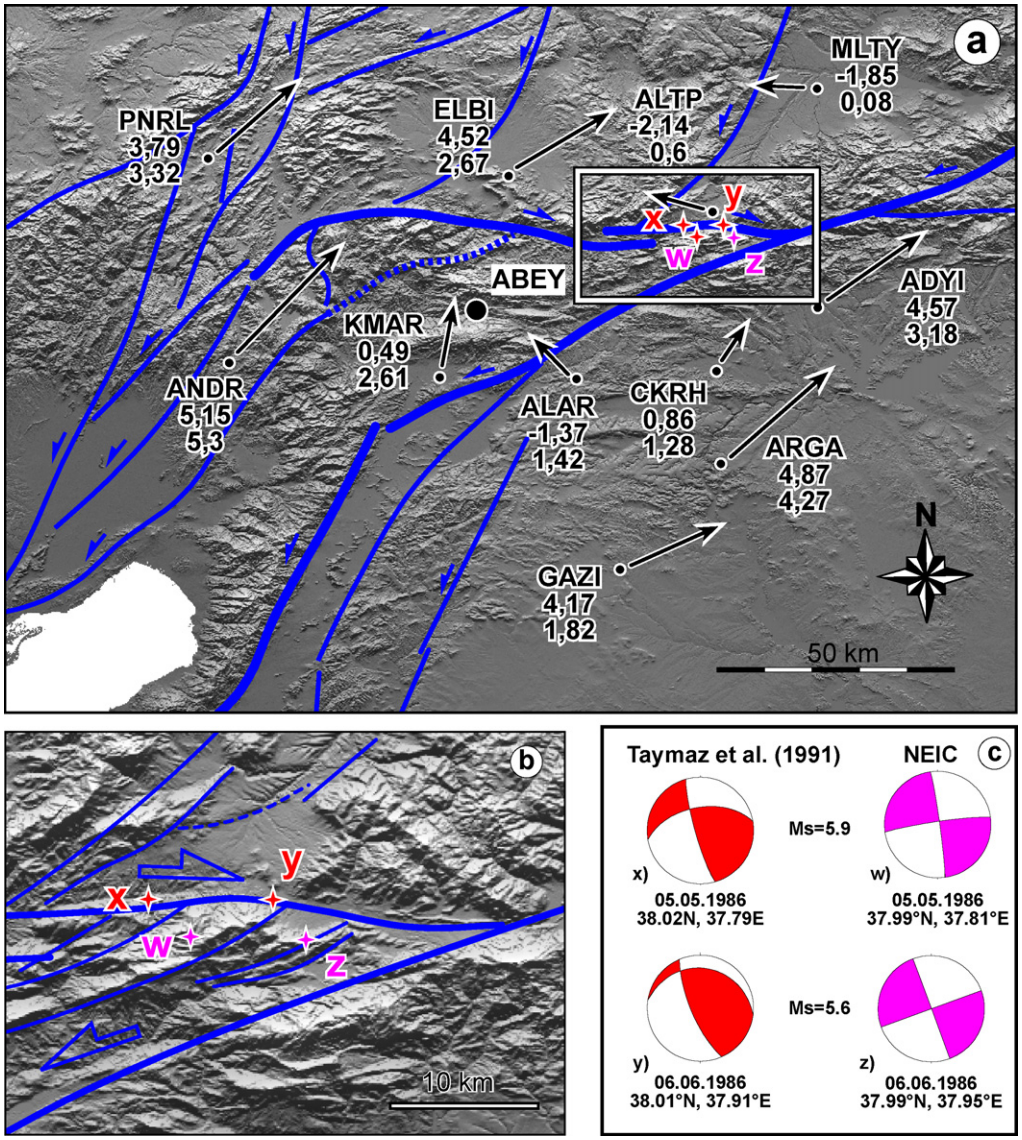

Fig. 12. (a) Simplified tectonic map and GPS vectors re-calculated according to ABEY station. (b) Close up figure for indicating proposed epicenter positions (*x*–*z*) and (c) corresponding moment tensor solutions (after Taymaz et al., 1991 and USGS-NEIC).

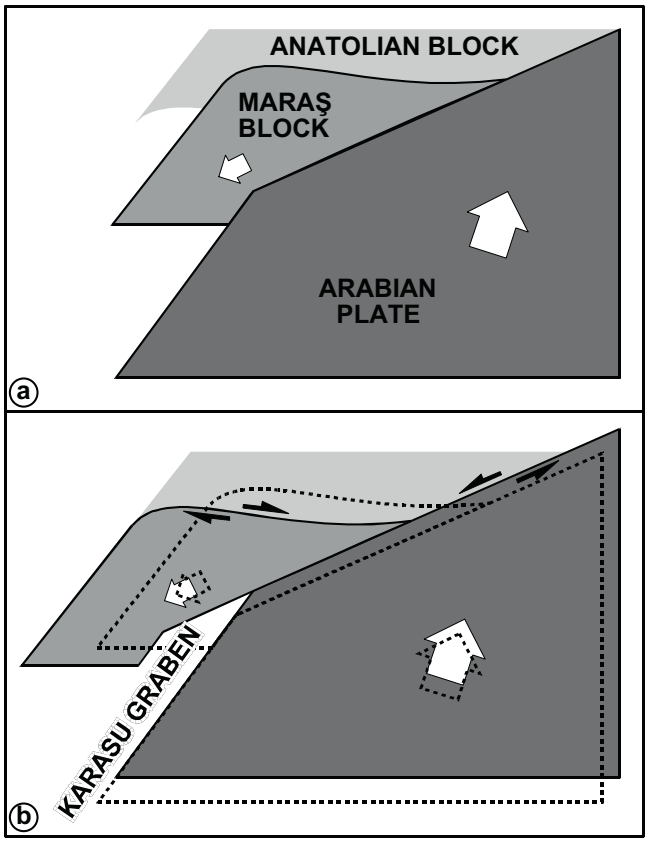

Fig. 13. Deformation model explaining the dextral motion of Sürgü Fault Zone. (a) Initial condition. (b) Present configuration (Anatolian Block taken as fixed). As the Arabian Plate and Anatolian Block converge, the squeezed Maraş Block caught between these landmasses escapes westward resulting in dextral motion between Maraş and Anatolian blocks while the relative motions between Arabian Plate and all other blocks are sinistral.

blocks and the delimiting normal faults show a staircase geometry consistent with domino-style faulting (Wernicke and Burchfield, 1982; Ron et al., 1984) along dextral strike slip SFZ that would result in clockwise block rotations (Fig. 11b and c). It is also worth noting that the faults between blocks have opposite senses of shear, as predicted, which is compatible with the sinistral EAFZ (Fig. 11b and c).

In addition to remote sensing and field based data, the GPS vectors provided by Reilinger et al. (2006) were re-calculated with respect to GPS stations located close to the center of the SFZ and located within the southern block (ABEY in Fig. 12a). Although, the density of the GPS stations is not adequate to determine convincingly the slip sense of the Sürgü Fault Zone, the GPS vectors with respect to Ağabeyli (ABEY) station show some correlation with the main tectonic features. As seen in Fig. 12 the Kahramanmaraş (KMAR) station indicates northward directed shortening of the area while Elbistan (ELBI) station clearly implies dextral movement along the SFZ. With the exception of the Çakırhöyük (CKRH) station, all the stations on the Arabian Block indicate a sinistral nature for the East Anatolian Fault Zone.

During the instrumental period, two moderate size earthquakes occurred in 1986 May 5 (Ms = 5.9) and 1986 June 6 (Ms = 5.6) in the region (Fig. 12b). The focal mechanism solutions of these earthquakes proposed by the Taymaz et al. (1991) indicate that the SFZ is a sinistral strike-slip fault zone. This contradicts observations presented in this paper and the results of the present stress analyses. The epicenters of these events are located at the intersection of SFZ and the Malatya Fault Zone (Fig. 12c). The earthquake data were recorded in 1986 when the number of recording stations was few and further from the epicenter than now. Therefore, these poorly located events alternatively might belong to Malatya or East Anatolian fault zones rather than SFZ, which would be consistent with the present results. For a more precise correlation, these events should be re-located.

4.2. Preferred block model

As discussed above, the dextral nature of the SFZ cannot be explained as a simple antithetic fault since the angle between EAFZ and SFZ is very narrow compared to the one predicted in the Riedel deformation pattern for shear zones (Fig. 1a). Possible explanations of this type fault geometry include rotation of early formed Coulomb fractures or reactivation of a pre-existing structure. Alternatively, Yin and Taylor (2012) suggested distributed deformation during the formation of adjoining shear zones with opposing senses of shear as a possible mechanism for the odd geometries of the conjugate strike-slip fault system in central Tibet. In this respect, the dextral nature of the SFZ can be explained by the northward (NNE) convergence of Arabian Plate (AP) forcing the wedge-shaped Maraş Block (MB) westward with respect to the Anatolian Block (AB) (Fig. 13). This movement is accommodated in the southeast by sinistral motion between AP and MB, and in the north by dextral motion between AB and MB. This evolutionary block model also predicts rifting between the EAFZ in the west and Dead Sea Fault Zone in the east, compatible with the opening of the Plio-Quaternary Karasu Rift (Boulton, 2007; Rojay et al., 2001; Parlak et al., 1998).

5. Conclusions

Remote sensing analysis, fieldwork and fault slip data all indicate the SFZ as a dextral strike-slip fault zone. This conclusion challenges almost all previous work defining the Sürgü Fault as a sinistral strike-slip fault (Perinçek et al., 1987; Taymaz et al., 1991; Şaroğlu et al., 1992).

The other conclusions of this study are as follows:

- Field observations and analysis of fault slip data indicate a strong reverse slip component at the west end of the SFZ (Göksun segment), where the fault geometry bends noticeable toward the south acting as a restraining bend.
- In the east, the SFZ is characterized by significant normal slip component and displays staircase fault morphology bounding wedge-shape basins such as Kozaklı Basin, consistent with dextral motion related clockwise block rotation in the southern block.
- Horizontal component of the calculated maximum compressive stress near the SFZ rotates with the curved geometry of the fault and makes an approximately 45° angle with the master strand. Compatibility between the fault geometry and local stress distribution clearly indicates that the resultant stress direction is currently valid.
- Observed maximum dextral cumulative off-set along the SFZ is about 3 km since the development of the current stream network.
- Dextral motion of SFZ identified in this study can be explained by westward escape of MB being squeezed between the N–S converging Arabian Plate and Anatolian Block.

In this study, the kinematic characteristics of the SFZ have been documented and a tectonic block model proposed to explain its dextral motion. However, there are some incomplete or conflicting points with the previous works. In order to solve these problems, further detailed geodetic, seismic and geological studies focused on the current movement of SFZ and paleomagnetic analysis are recommended in order to test the proposed block rotation model.

Acknowledgements

Research for this paper was supported by ÖYP research foundation No: BAP-08-11-DPT.2002K120510 and Middle East Basins Evolution (MEBE) program. We would like to express our special thanks to Dr. A. Arda Özacar who evaluated the moment tensor solutions of the earthquakes occurred in the region and also for his invaluable and critical comments that greatly improved an earlier version of this manuscript. Two anonymous reviewers are also acknowledged for their constructive comments.

References

Ambraseys, N.N., Tchalenko, J.S., 1970. The Gediz (Turkey) earthquake of March 28. Nature 227, 592–593.
Anderson, E.M., 1951. The Dynamics of Faulting, second ed. Oliver and BoydEdinburgh.
Angelier, J., 1979. Determination of the mean principal directions of stresses for a given fault population. Tectonophysics 56 (3–4), T17–T26.
Angelier, J., 1984. Tectonic analysis of fault slip data sets. Journal of Geophysical Research 89 (B7), 5835–5848.
Angelier, J., 1988. TECTOR: Software for Palaeostress Inversion: Quantitative Tectonics. University of P.M. Paris 5.
Angelier, J., 1990. Inversion of field data in fault tectonics to obtain the regional stress. III. A new rapid direct inversion method by analytical means. Geophysical Journal International 103, 363–376.
Angelier, J., 1994. Fault slip analysis and palaeostress reconstruction. In: Hancock, P.L. (Ed.), Continental Deformation. Pergamon Press, Oxford, pp. 53–101.
Arpat, E., 1972. The East Anatolian Fault System: troughs on its development: MTA Bulletin, Ankara, 78, pp. 33–39.
Arpat, E., Şaroğlu, F., 1975. Türkiye'deki bazı önemli genç tektonik olaylar. Bulletin of the Geological Society of Turkey 18, 91–101.
Barrier, E., Vrielynck, B., 2008. MEBE Atlas of Paleotectonic Maps of the Middle East. Commission for the Geological Map of the World.
Biddle, K.T., Christie-Blick, N., 1985. Deformation and basin formation along strike-slip faults. In: Biddle, K.T., Christie-Blick, N. (Eds.), Strike-slip Deformation, Basin Formation and Sedimentation. Spec. Publ. Soc. Econ. Paleont. Miner. 37, 1–45.
Biryol, C.B., Beck, S.L., Zandt, G., Ozacar, A.A., 2011. Segmented African lithosphere beneath the Anatolian region inferred from teleseismic P-wave tomography. Geophysical Journal International 184, 1037–1057.
Bott, M.P.H., 1959. The mechanics of oblique-slip faulting. Geological Magazine 96, 109–117.
Boulton, S.J., 2007. New insights into the northern Dead Sea Fault Zone (Karasu Rift and Hatay Graben), Southern Turkey. American Geophysical Union, Fall Meeting.
Cunningham, W.D., Mann, P., 2007. Tectonics of strike-slip restraining and releasing bends. Geological Society, London, Special Publications 290, 1–12.
Dewey, J.F., Sengör, A.M.C., 1979. Aegean and surrounding regions: complex multiplate and continuum tectonics in a convergent zone. Geological Society of America Bulletin 90 (I), 84–92.
Dewey, J.F., Hempton, M.R., Kidd, W.S.F., Saroglu, F., Şengör, A.M.C., 1986. Shortening of continental lithosphere: the Neotectonics of Eastern Anatolia—a Young Collision Zone. Collision Tectonics, Geological Society Special Publication 19, 3–36.
Dewey, J.F., Holdsworth, R.E., Strachan, R.A., 1995. Transpression and transtension zones. Geological Society, London, Special Publications 135, 1–14.
Faccenna, C., Bellier, O., Martinod, J., Piromallo, C., Regard, V., 2006. Slab detachment beneath eastern Anatolia: a possible cause for the formation of the North Anatolian Fault. Earth and Planetary Science Letters 242, 85–97.
Gans, C.R., Beck, S.L., Zandt, G., Biryol, C.B., Ozacar, A.A., 2009. Detecting the limit of slab break-off in central Turkey: new high-resolution Pn tomography results. Geophysical Journal International 179, 1566–1572.
Govers, R., Wortel, M.J.R., 2005. Lithosphere tearing at STEP faults: response to edges of subduction zones. Earth and Planetary Science Letters 236, 505–523.
Ghasemi, A., Talbot, C.J., 2005. A new tectonic scenario for the Sanandaj–Sirjan Zone (Iran). Journal of Asian Earth Sciences 26, 683–693.
Hüsing, S.K., Zachariasse, W.J., van Hinsbergen, D.J.J., Krijgsman, W., Inceöz, M., Harzhauser, M., Mandic, O., Kroh, A., 2009. Oligo-Miocene foreland basin evolution in SE Anatolia: constraints on the closure of the eastern Tethys gateway. In: van Hinsbergen, D.J.J., Edwards, M.A., Govers, R. (Eds.), Collision and Collapse at the Africa-Arabia-Eurasia Subduction Zone. Geological Society, London, Special Publication. , pp. 107–132.
Jaeger, J., Cook, N.G.W., 1971. Fundamentals of Rock Mechanics. Chapman and Hall, London.
Kaymakci, N., De Bruijn, H., White, S.H., Van Dijk, M., Saraç, G., Unay, E., 2001. Tectonic implications of the Neogene stratigraphy of the Çankiri basin with special reference to the Çandir locality (North-Central Anatolia, Turkey). In: Güleç, E., Begun, D.R., Geraads, D. (Eds.), Geology and Vertebrate Paleontology of the Miocene hominoid locality of Çandir. Courier Forschungsinstitut Senckenberg 240, pp. 9–28.
Kaymakci, N., Duermeijer, C.E., Langereis, C., White, S.H., van Dijk, P.M., 2003. Oroclinal bending due to indentation: a paleomagnetic study for the early Tertiary evolution of the Çankırı Basin (Central Anatolia Turkey). Geological Magazine 140, 343–355.
Kaymakci, N., Inceöz, M., Ertepinar, P., 2006. 3D architecture and Neogene evolution of the Malatya Basin: inferences for the kinematics of the Malatya and Ovacik Fault Zones. Turkish Journal of Earth Sciences 15, 123–154.
Kaymakci, N., Inceöz, M., Ertepinar, P., Koç, A., 2010. Late Cretaceous to recent kinematics of SE Anatolia (Turkey). In: Sosson, M., Kaymakci, N., Stephenson, R., Starostenko, V., Bergerat, F. (Eds.), Sedimentary Basin Tectonics from the Black Sea and Caucasus to the Arabian Platform. Geological Society London Special Issue No. 340, pp. 409–435.
Kaymakci, N., Özçelik, Y., White, S.H., van Dijk, P.M., 2009. Tectono-stratigraphy of the Çankiri Bas: late Cretaceous to early Miocene evolution of the Neotethyan suture zone in Turkey. In: van Hinsbergen, D.J.J., Edwards, M.A., Govers, R. (Eds.), Collision and Collapse at the Africa-Arabia-Eurasia Subduction Zone. Geological Society of London Special Publication. , pp. 67–106.
Keskin, M., 2003. Magma generation by slab steepening and breakoff beneath a subduction-accretion complex: an alternative model for collision-related volcanism in Eastern Anatolia, Turkey. Geophysical Research Letters 30 (24), 8046, http://dx.doi.org/10.1029/2003GL018019.
Khair, K., Tsokas, G.N., 1999. Nature of the Levantine (eastern Mediterranean) crust from multiple-source Werner deconvolution of Bouguer gravity anomalies. Journal of Geophysical Research 104, 25469–25478.
Kozlu, H.,1987. Structural development and stratigraphy of Misis-Andirin Region. In: 7th Biannual Petroleum Congress of Turkey. UCTEA Chamber of Petroleum Engineers-Turkish Association of Petroleum Geologist, pp. 104–116.
Krantz, R.W., 1988. Multiple fault sets and three-dimensional strain: theory and application. Journal of Structural Geology 10 (3), 225–237.
Lyberis, N., Yurur, T., Chorowicz, J., Kasapoglu, E., Gündoğdu, N., 1992. The East Anatolian Fault: an oblique collisional belt. Tectonophysics 204, 1–15.
Muehlberger, W.R., Gordon, M.B., 1987. Observations on the complexity of the East Anatolian Fault, Turkey. Journal of Structural Geology 9 (7), 899–903.
Naylor, M.A., Mandl, G., Sijpesteijn, C.H.K., 1986. Fault geometries in basement-induced wrench faulting under different initial stress states. Journal of Structural Geology 8, 737–752.
Okay, A.I., Zattin, M., Cavazza, W., 2010. Apatite fission-track data for the Miocene Arabia-Eurasia collision. Geology 38, 35–38.
Parlak, O., Kop, A., Ünlügenç, U.C., Demirkol, C., 1998. Geochronology and geochemistry of basaltic rocks in The Karasu Graben Around Kırıkhan (Hatay), S. Turkey. Turkish Journal of Earth Sciences 7, 53–61.
Perincek, D., Çemen, I., 1990. The structural relationship between the East Anatolian and Dead Sea fault zones in southeastern Turkey. Tectonophysics 172, 331–340.
Perinçek, D., Kozlu, H., 1984. Stratigraphy and structural relations of the units in the Afsin-Elbistan-Doganshehir region (Eastern Taurus). In: Tekeli, O., Göncüoglu, M.C. (Eds.), Geology of the Taurus Belt. General Directorate of Mineral Research and Exploration (MTA) Special Publication. , pp. 181–198.
Perinçek, D., Günay, Y., Kozlu, H.,1987. New observations on strike-slip faults in East and Southeast Anatolia. In: 7th Biannual Petroleum Congress of Turkey. UCTEA Chamber of Petroleum Engineers-Turkish Association of Petroleum Geologist, pp. 89–103.
Reches, Z., 1978. Analysis of faulting in three-dimensional strain field. Tectonophysics 47 (1–2), 109–129.
Reches, Z., 1983. Faulting of rocks in three-dimensional strain fields. II. Theoretical analysis. Tectonophysics 95 (1–2), 133–156.
Reilinger, R., McClusky, S., Vernant, P., Lawrence, S., Ergintav, S., Cakmak, R., Nadariya, M., Hahubia, G., Mahmoud, S., Sakr, K., ArRajehi, A., Paradissis, D., Al-Aydrus, A., Prilepin, M., Guseva, T., Evren, E., Dmitritsa, A., Filikov, S.V., Gomes, F., Al-Ghazzi, R., Karam, G., 2006. GPS constraints on continental deformation in the Africa-Arabia-Eurasia continental collision zone and implications for the dynamics of plate interactions. Journal of Geophysical Research 111, V05411, doi:05410.01029/02005JB004051.
Robertson, A.H.F., Ustaömer, T., Parlak, O., Ülüngenç, U.C., Tasli, K., Nurdan, I., 2006. The Berit transect of the Tauride thrust belt, S Turkey: Late Cretaceous-Early Cenozoic accretionary/collisional processes related to closure of the Southern Neotethys. Journal of Asian Earth Sciences 27, 108–145.
Rojay, B., Heimann, A., Toprak, V., 2001. Neotectonic and volcanic characteristics of the Karasu fault zone (Anatolia, Turkey): The transition zone between the Dead Sea transform and the East Anatolian fault zone. Geodinamica Acta 14, 1–17.
Rolland, Y., Perincek, D., Kaymakci, N., Sosson, M., Barrier, E., 2012. Evidence for ~80–75 Ma subduction jump during Anatolide-tauride-Armenian block accretion and ~48 Ma Arabian-Eurasioan collision in Lesser Caucasus-East Anatolia. Journal of Geodynamics 56, 76–85.
Ron, H., Freund, R., Garfunkel, Z., Nur, A., 1984. Block rotation by strike slip faulting: structural and palaeomagnetic evidence. Journal of Geophysical Research 89, 6256–6270.
Sanderson, D., Marchini, R.D., 1984. Transpression. Journal of Structural Geology 6, 449–458.
Şaroğlu, F., Emre, Ö., Kuşçu, I., 1992. The East Anatolian Fault Zone of Turkey. Annale Tectonicae. Special Issue-Supplement to Volume VI, pp. 99–125.
Segall, P., Pollard, D.D., 1983. Nucleation and growth of strike slip faults in granite. Journal of Geophysical Research 88, 555–568.
Şengör, A.M.C., Yılmaz, Y., 1981. Tethyan evolution of Turkey: a plate tectonic approach. Tectonophysics 75, p181–p241.
Şengör, A.M.C., Görür, N., Şaroğlu, F., 1985. Strike-slip faulting and related basin formation in zones of tectonic escape: Turkey as a case study. In: Biddle, K.T., Christie-Blick, N. (Eds.), Basin Formation and Sedimentation. Society of Economic Paleontologists and Mineralogists Special Publications 37. , pp. 227–264.

Şengör, A.M.C., 1987. Cross-faults and differential stretching of hanging walls in regions of low-angle normal faulting: examples from western Turkey. Geological Society, London, Special Publications 28, 575–589.
Şengör, A.M.C., Özeren, S., Genç, T., Zor, E., 2003. East Anatolian high plateau as a mantle-supported, north-south shortened domal structure. Geophysical Research Letters 30 (24), 8045, http://dx.doi.org/10.1029/2003GL017858.
Sylvester, A.G., 1988. Strike-slip Faults. GSA Bulletin 100, pp. 1666–1703.
Taymaz, T., Eyidoğan, H., Jackson, J., 1991. Source parameters of large earthquakes in the East Anatolian Fault Zone (Turkey). Geophysical Journal International 106 (3), 537–550.
Van Hinsbergen, D.J.J., Kaymakci, N., Spakman, W., Torsvik, T.H., 2010. Reconciling the geological history of western Turkey with plate circuits and mantle tomography. Earth and Planetary Science Letters 297, 674–686.
Wallace, R.E., 1951. Geometry of shearing stress and relation to faulting. Journal of Geology 69, 118–130.
Wernicke, B., Burchfield, B.C., 1982. Modes of extensional tectonics. Journal of Structural Geology 4, 105–115.
Westaway, R., Demir, T., Seyrek, A., Beck, A., 2006. Kinematics of active left-lateral faulting in SE Turkey from offset Pleistocene river gorges: improved constraint on the rate and history of relative motion between the Turkish and Arabian plates. Journal of the Geological Society 163, 149–164.
Wilcox, R.E., Harding, T.P., Seely, D.R., 1973. Basic wrench tectonics. American Association of Petroleum Geologist Bulletin 57, 74–96.
Woodcock, N.H., Fischer, M., 1986. Strike-slip duplexes. Journal of Structural Geology 8, 725–735.
Yin, A., Taylor, M.H., 2012. Mechanics of V-shaped conjugate strike-slip faults and the corresponding continuum mode of continental deformation. Geological Society of America Bulletin 123 (9–10), 1798–1821, doi:10.1130/B30159.1.
Yurtmen, S., Guillou, H., Westerman, R., Rowbotham, G., Tatar, O., 2002. Rate of strike slip motion on the amanas fault (Karasu Valley, Southern Turkey) constrained by K-Ar dating and geochemical analysis of quaternary basalts. Tectonophysics 344, 207–246.